Fibers and Polymers (2024) 25:3185–3199
https://doi.org/10.1007/s12221-024-00645-x

Online ISSN 1875-0052
Print ISSN 1229-9197

REGULAR ARTICLE

Prediction of Macroscopic Compressive Mechanical Properties for 2.5D Woven Composites Based on Artificial Neural Network

Jie Zhou[1] · Haolin Wei[1] · Zhen Wu[1,2] · Zhengliang Liu[1] · Xitao Zheng[1,2]

Received: 29 April 2024 / Revised: 4 July 2024 / Accepted: 12 July 2024 / Published online: 24 July 2024

Abstract
The complex modeling and computational cost are unavoidable in analysis of finite element models (FEMs) when mechanical properties of woven composite materials are predicted. To overcome the drawbacks of FEMs, two different artificial neural network models (ANNMs) based on quasi-static axial compression experimental data of 2.5D woven composite plates (2.5DWCPs) are constructed: (1) The direct strength prediction model (DSPM) is a non-destructive way to predict strength, which is meaningful in engineering; (2) The indirect strength prediction model (ISPM) is based on stress–strain curves, which firstly proposes a simplified data processing method including the state variables (SVs). The SVs are introduced to modify the experimental stress–strain curves, which not only reduces training data size but also significantly improves prediction accuracy. Then, the performance of the DSPM and the ISPM has been evaluated by numerical examples. The results indicate that the DSPM has simple and direct expressions of input parameters (IPs) and output parameters (OPs), which makes it easier to construct and train ANNMs. The ISPM not only utilizes sufficient training data from experiments but also performs well in predicting stress–strain curve and failure strain. In short, two proposed ANNMs have ability to fast and accurately predict compression strength, which are more suitable for engineering than FEMs. To reduce experimental costs, the DSPM is proposed to produce reasonable results. If a lot of experimental data are prepared, the ISPM can produce more accurate results.

Keywords 2.5D woven composites · Artificial neural network · Compression strength · Failure strain

1 Introduction

Composite materials are widely used in various aerospace equipment [1] due to their excellent characteristics such as low specific weight, high specific strength and large specific modulus [2]. Three-dimensional (3D) woven composites have a complex interlocking structure in space network, which overcomes the weakness of traditional composite laminates such as weak interlayer performance and poor impact resistance [3]. What's more, it has strong designability and excellent mechanical properties, which is more suitable for engineering applications. At present, the weaving process of most 3D woven composites cannot be separated from manual assistance. However, as a kind of 3D woven composites, the automated manufacturing process of 2.5D (three-dimension angle-interlock) [4] woven composites is more perfect. Therefore, 2.5D woven composite plates (2.5DWCPs) is more widely used because it has advantages of low cost and easy preparation [5].

To take full advantage of the potentials of 2.5DWCPs, many investigators have proposed abundant analytical models and finite element models (FEMs) to accurately predict the mechanical properties of 2.5DWCPs. Kang et al. [6] developed the Eshelby-Mori-Tanaka inclusion theory and the stiffness volume average method to predict the effective properties of polymer composite reinforced by fiber-rod and 3D weavings (PCFR3DWs). To avoid geometry modeling and meshing of complex reinforcements and matrix regions in textile composites, the fiber-reinforced voxel modeling technique is proposed by Xie et al. [7]. This technique can accurately analyze stress fields and predict the stiffness of textile composites. What's more, Zhang et al. [8] proposed a meso-scale voxel-based model established by the measured parameters from the CT image, which is capable of accurately predicting mechanical properties of warp-reinforced

✉ Zhen Wu
wuzhenhk@nwpu.edu.cn

1 School of Aeronautics, Northwestern Polytechnical University, Xian 710072, China

2 National Key Laboratory of Strength and Structural Integrity, Xi'an 710065, China

2.5D woven composites. Hallal et al. [9] proposed an analytical model to predict the effective elastic properties for 2.5DWCPs, in which three-stages homogenization method (3SHM) was adopted. Yao and Liu et al. [10] estimated the mechanical properties of 2.5D woven SiO_2f/SiO_2 ceramic matrix composite by using stiffness averaging methods (SAMs). A semi-analytical method has been proposed by Chen et al. [4] to express elastic constants in terms of microstructure geometrical parameters and constitute properties, which is applied to predict elastic constants of 2.5D continue carbon fiber reinforced silicon carbide (C/SiC) composites. Based on a meso-scale representative volume element (RVE) model, Liu et al. [11] established a macro-scale progressive damage model to analyze the damage behaviors of 3D angle-interlock woven composites under uniaxial tension. In addition, Younes and Zaki [12] optimized the RVE of 2.5D interlock composites to enhance damage resistance and elastic stiffness. Due to their complicated macro/micro structure, however, it is difficult to analyze 2.5D/3D woven composite materials using the FEMs. The FEMs not only have complex modeling process but also require to obtain material properties such as elastic modules, strength and failure modes by different kinds of mechanical experiments. Therefore, investigators attempted to explore novel methods to research the issues encountered in FEMs.

In the process of studying mechanical properties and failure modes of 2.5DWCPs, it is difficult to accurately predict the strength of 2.5DWCPs with angle-ply woven laminas because of the obvious nonlinear phenomenon in quasi-static experiments. What's more, the tension tests along the warp and weft directions have been conducted by Ma et al. [13], in which it was found that the stress–strain curves exhibit mostly nonlinear behaviors. Odegard et al. [14] developed a FEM to predict the nonlinear response of 8HS woven graphite/PMR-15 composite material subjected to shear-dominated biaxial loads. Ogihara and Reifshider [15] investigated nonlinear stress–strain behavior in woven glass/epoxy laminates under off-axis tension by experiments. Moreover, the one-parameter plasticity model was established to predict the nonlinear effect. Cousigne et al. [16] developed a nonlinear material model for thick shells of textile composite materials, which has been evaluated by tension and compression tests on plain and twill weave carbon fiber composites. By combining plain-woven RVE and a nonlinear three-phase bridging model, Wang et al. [17] presented an analytical model to describe the nonlinear behavior of a plain-woven composite under off-axis loads. To sum up, the nonlinear effect is non-negligible in the predicting mechanical properties of 3D woven composite materials.

With the rapid development of high-performance computers and data-driven analysis in recent years, machine learning algorithms (MLAs) have been applied widely in various fields [18]. The MLAs not only extract useful physical characteristics from massive experimental data but also directly predict mechanical properties of composite materials without complex modeling and analysis in FEM [19, 20]. Zhang et al. [21] presented a method based on MLA and FEM to predict the strength and progressive damage behavior of carbon fiber-reinforced polymer (CFRP) laminates with holes. Sharan and Mitra [22] developed an ANN model with significant parameters affecting the strength properties of CFRP laminates, and the hyper-parameter of the ANN model has been optimally selected. Kim et al. [23] combined principal component analysis (PCA) with deep neural network (DNN) to build the data-driven model, which can efficiently predict the stress–strain curves of unidirectional (UD) composites. ANN model was developed by Gowid et al. [24] to predict the high nonlinear crushing behavior of plain weave composite hexagonal quadruple ring system (CHQRS). Liu et al. [25] proposed a micromechanical model by mechanics of structure genome (MSG) and DNN model, which can capture the failure initiation at the fiber and matrix level in textile composites. Halvaei et al. [26] investigated the flexural load and toughness of carbon woven textiles with different mesh sizes and volume percentages. They developed an ANN model to predict the flexural strength of the carbon textile reinforced concrete samples. However, the cost of a large number of experiments is very expensive, and it is difficult to satisfy the requirements in engineering. In addition, the integrity and richness of training datasets obtained from experiments cannot be ensured. Therefore, most datasets in existing investigations origin from the results of numerical simulation in FEMs.

By reviewing the literature, it is found that the complex modeling and computational cost are unavoidable in the analysis of FEMs when mechanical properties of woven composite materials are predicted. However, the MLAs have the advantage of processing data. To overcome the drawbacks of FEMs, two different ANNMs based on quasi-static axial compression experimental data of 2.5DWCPs are constructed. To reduce experimental costs, this work firstly attempts to construct the direct strength prediction model (DSPM), in which input parameters (IPs) and output parameters (OPs) have direct expression. Thus, it is more convenient to train ANNMs. In addition, a number of stress–strain curves have been obtained in present experiment. To effectively utilize these experimental data, the indirect strength prediction model (ISPM) has been also constructed. Due to involvement of rich experimental data, the ISPM is more accurate in predicting compression strength. However, for the ISPM, the sudden stress drop will significantly influence the prediction accuracy. To avoid such issue, a data reduction method is firstly proposed. Therefore, the modified ISPM can be suggested to accurately predict stress–strain curve and failure strain, when sufficient data have been obtained. The specific technology research roadmap is shown in Fig. 1.

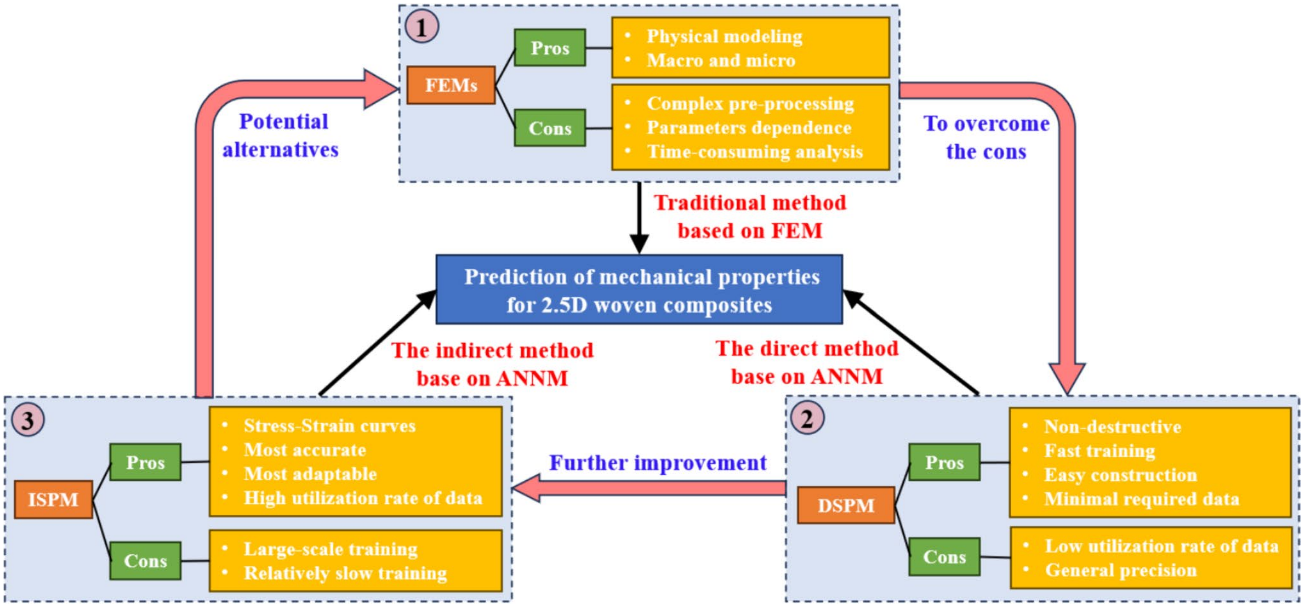

Fig. 1 The technology research roadmap in present work

Table 1 Details on different types of 2.5DWCPs

Plate ID	Weaving scheme	Thickness/mm	Quantity
A0	$[90/\pm 45/\overline{90}]_S$	3.59	5
A1	$[90/\pm 63.43/\overline{90}]_S$	4.56	5
B0	$[90/45/0/-45/\overline{90}]_S$	4.31	5
B1	$[90/63.43/0/-63.43/\overline{90}]_S$	5.28	7
C	$[90/0/\pm 45/0/\overline{90}]_S$	5.05	7

2 Compression Experiments

CCF800H/5284 was selected as the raw material for weaved composite. M2.5D weaving process and RTM molding techniques were applied in manufacture. The details of the weaving scheme, geometric dimension and quantity of test specimen are shown in Table 1. A0 and A1 have a similar stacking sequence and different angle-ply weaved laminas. B0 and B1 insert cross-ply weaved laminas based on A0 and A1. C changes the stacking sequence of cross-ply and angle-ply weaved laminas compared with A0 and B0.

The warp compression experiments of weaved composite specimen can refer to ASTM D6641 standard. The compression experimental data were obtained from five types of 2.5DWCPs, which include 29 specimens in total. The nominal length of specimen is 140mm and the nominal width of the specimen is 12 mm. The nominal thickness of specimen is presented in Table 1. Each specimen was measured before compression experiment. Figure 2 shows the average geometric parameters of 2.5D woven composites.

Figure 3a and b present the measurement process and the whole testbench of the specimen, respectively. The displacement loading mode was adopted in experiment and the test loading rate is 0.5mm/min. The compressive elastic moduli of five different types of 2.5DWCPs were measured. In addition, the ultimate failure loads and failure modes of specimens were acquired. The DH3820 static strain test system was used to record the strain changes during experiments. Finally, the experimental results of 29 stress–strain curves were obtained. For further analysis, the stress–strain curves and damaged specimens of five different types of 2.5DWCPs obtained from the compression experiment are all shown in Fig. 4.

Based on the stress–strain curves obtained from experiments, the specific initial elastic modulus and compression strength of five types of 2.5DWCPs are presented in Fig. 5. The average initial moduli of A0, A1, B0, B1 and C type woven composite plates are 19.02, 8.28, 38.57, 24.77 and 53.84 GPa. The average strength of A0, A1, B0, B1 and C type woven composite plates are 141.91, 178.93, 224.02, 185.19 and 304.10 MPa.

3 Stress Prediction Model Based on ANN

3.1 Basic Principle

ANN is one type of MLAs. The main feature of ANNs is that the network includes input, hidden and output layers. The

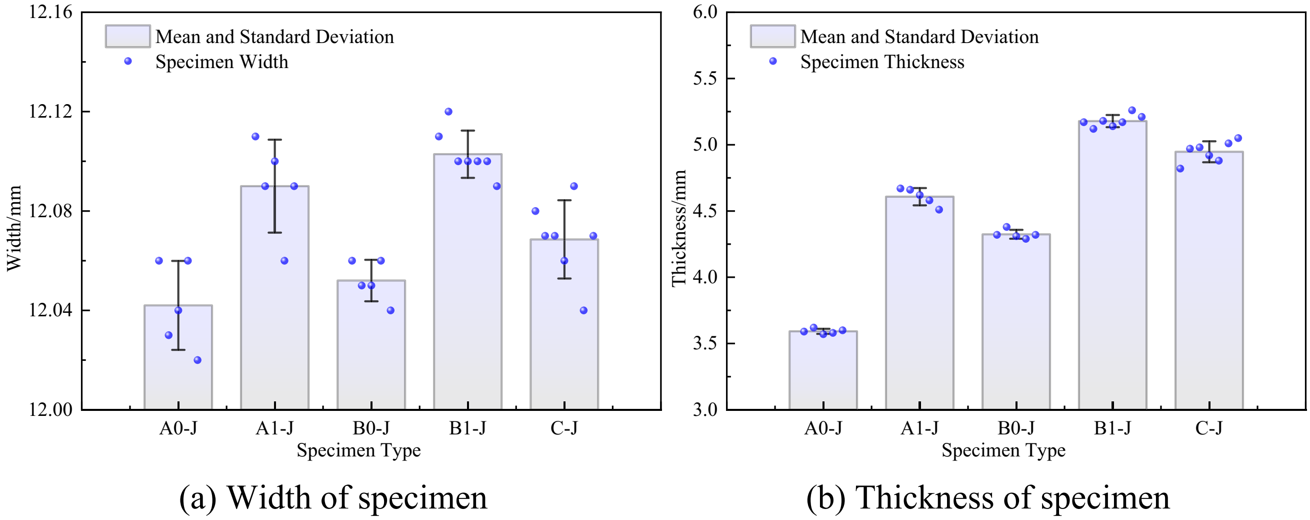

Fig. 2 The average geometric parameters of 2.5DWCPs

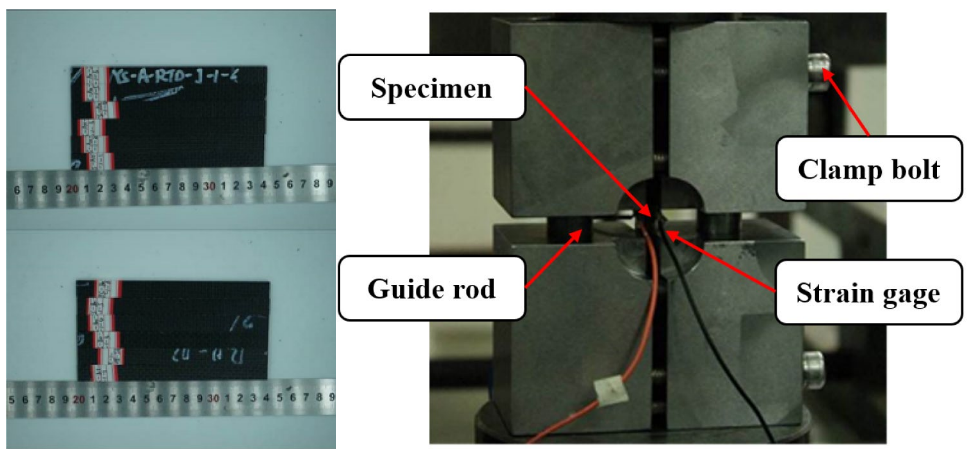

(a) Measurement of specimens (b) Testbench of specimen

Fig. 3 Preparation and testbench of compression experiment

number of different kinds of layers can be flexibly defined, which is commonly determined by complexity and scale of training data structures. The schematic of the ANN model is illustrated in Fig. 6. From the perspective of mathematic, ANN is composed of linear matrix operation and nonlinear activation function, which has a strong ability of characterization for data structures [27, 28].

The computational formula at each node of the hidden layers and output layers is presented as follows

$$O = f\left(\sum_{i=1}^{n} x_i w_i + b\right) \tag{1}$$

where O denotes the output of node i, x_i and w_i represent the output of all nodes in previous layer and corresponding weights, respectively. b is the bias of the previous layer. $f(x)$ signifies the activation function of neuron in hidden layers. The common activation functions [29, 30] include Softplus ($f(x) = \ln(1 + e^x)$), Sigmoid ($f(x) = 1/(1 + e^{-x})$) and ReLU ($f(x) = \max(0, x)$).

The training process for a concrete structure of a neural network means that the weight and bias should be updated to characterize the corresponding mapping relationship between input layers and output layers. During the training process, the weights and biases of each neuron in hidden layers are constantly adjusted by backpropagation (BP). The training of neural networks does not stop until the error between predictions and outputs reaches the preset convergence condition. The training process of ANN is shown in Fig. 7.

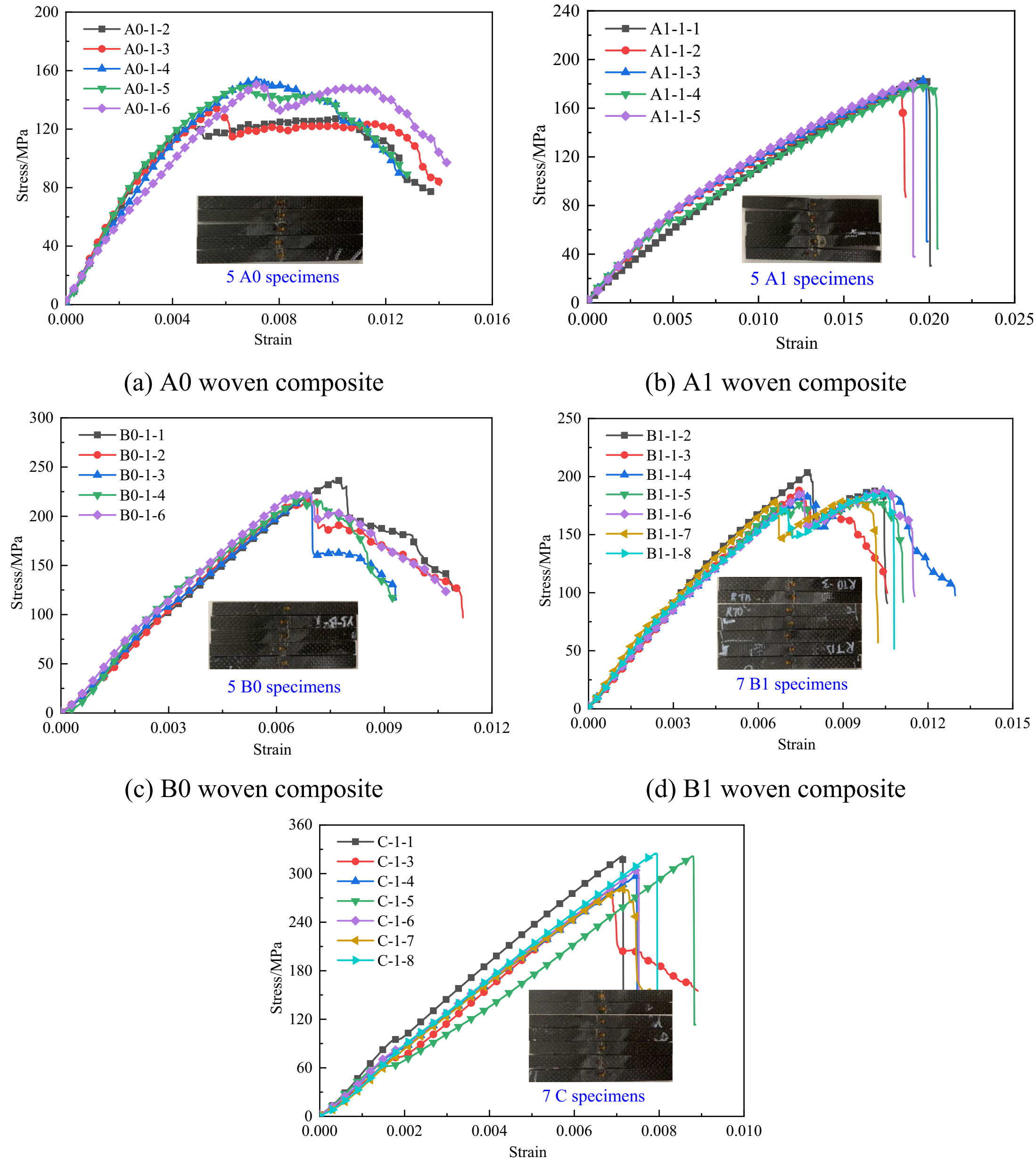

(a) A0 woven composite

(b) A1 woven composite

(c) B0 woven composite

(d) B1 woven composite

(e) C woven composite

Fig. 4 The stress–strain curves of 2.5DWCPs

3.2 Compression Strength Prediction Model

To predict compression strength in the warp direction of 2.5DWCPs with different stacking sequences, it is significant to determine the effective inputs of neural network. It is natural that the parameters containing information of stacking sequences and ply angles should be selected as IPs. However, five types of 2.5DWCPs have different layers and discontinuous ply angles. Therefore, the number of layers and angles of lamina are difficult to be directly utilized as IPs of ANNM.

Experiments and numerical analysis are two common methods to obtain the elastic moduli of 2.5DWCPs. The compression modules in the warp direction can be acquired by non-destructive compression experiments. What's more, SAM and FEM can also calculate compression modules. The elastic moduli of 2.5DWCPs is the simplest quantitative characterization for stacking sequences and ply angles. Therefore, the initial compression modules in the warp direction are selected as the first IP of ANNM.

Considering the slight nonlinear effects during the compression experiment, for the prediction of compression

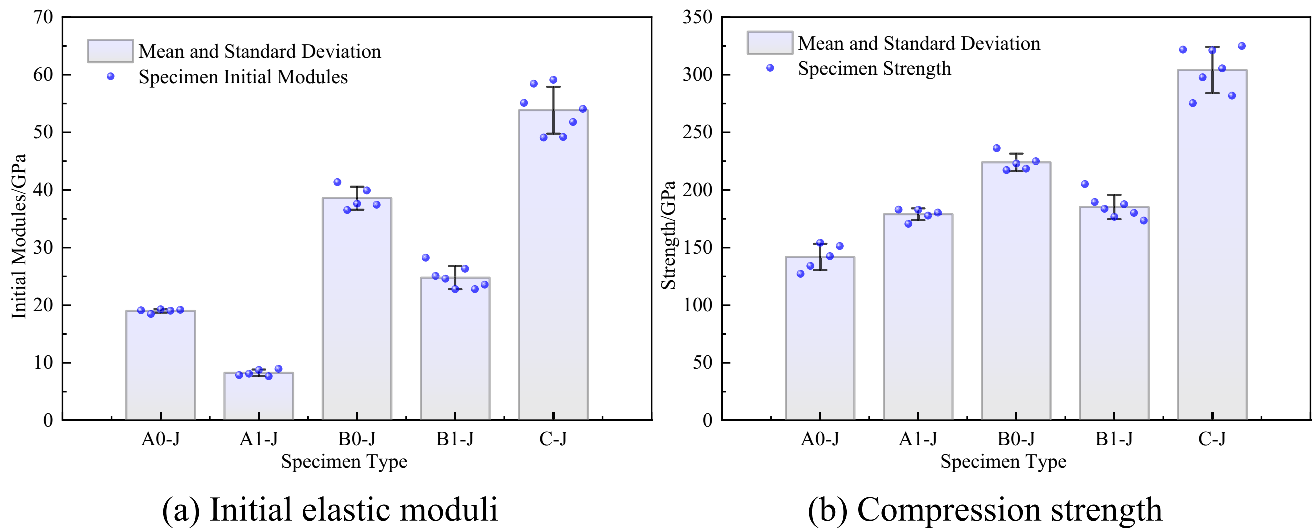

Fig. 5 The results of compression experiment for 2.5DWCPs

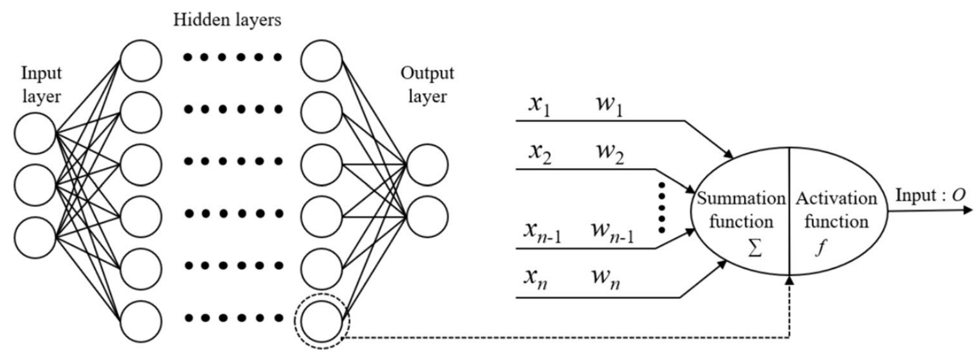

Fig. 6 The schematic of Artificial Neural Network Models (ANNMs)

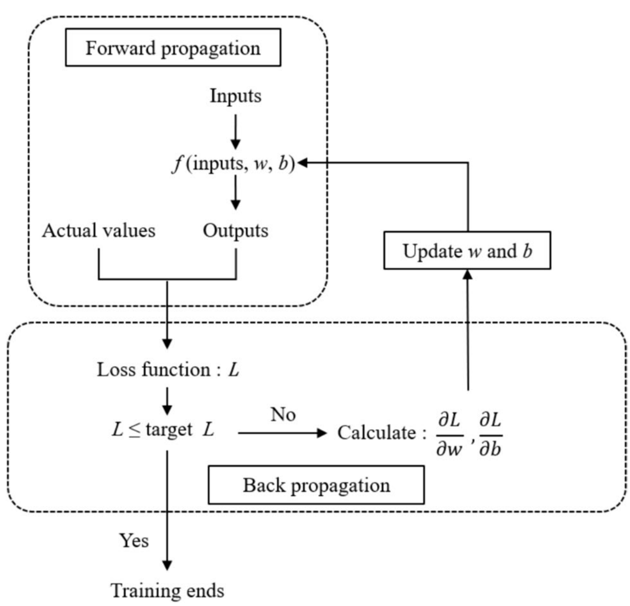

Fig. 7 Training process of Artificial Neural Network (ANN)

strength, the geometry dimensions of 2.5DWCPs are critical influence factors. The nominal lengths of five 2.5DWCPs are constant. In addition, the widths of 2.5DWCPs are nearly equal to 12mm, which are shown in Fig. 2a. The thickness of specimen changes with the type of 2.5DWCPs (A0, A1, B0, B1 and C), which is shown in Fig. 2b. In other words, the cross-sectional area of the compression specimen is mainly dominated by the thickness. Therefore, it is natural to set the thickness of specimen as the second IP of ANNM.

To illustrate more clearly the physical relationship between the selected IPs (the initial compression modules and the thickness of the specimen) and OP (the compressive strength), the stress–strain relationship in the warp compressive direction of 2.5DWCPs is presented in Eq. (2).

$$\sigma_{\mathrm{wc}} = E_{\mathrm{wc}}^{\mathrm{Eq}} \varepsilon_{\mathrm{wc}} \tag{2}$$

where the subscript ‘wc’ means the direction of warp compression and $E_{\mathrm{wc}}^{\mathrm{Eq}}$ means the equivalent modulus. In addition,

σ_{wc} and $\varepsilon_{\mathrm{wc}}$ denote stress and strain, respectively. By equivalent substitution, Eq. (3) can be obtained.

$$\begin{cases} \sigma_{\mathrm{wc}} = F_{\mathrm{wc}} \big/ A \\ \varepsilon_{\mathrm{wc}} = u_{\mathrm{wc}} \big/ L \\ A = W \cdot T \\ F_{\mathrm{wc}} = k_{\mathrm{wc}} \cdot u_{\mathrm{wc}} \end{cases} \rightarrow \frac{k_{\mathrm{wc}}}{W \cdot T} = \frac{E_{\mathrm{wc}}^{\mathrm{Eq}}}{L} \tag{3}$$

where A, W and T signify cross-sectional area, width and thickness of the specimen, respectively. L denotes the nominal length of the specimen. F_{wc} and u_{wc} denote the applied force and displacement, and k_{wc} denote the stiffness.

It must be noted that W and L are basically constant. Then, the three variables $E_{\mathrm{wc}}^{\mathrm{Eq}}$, T and k_{wc} can be utilized as input parameters for model training. As long as two of three variables are known, the third variable can be determined. It is clear that $E_{\mathrm{wc}}^{\mathrm{Eq}}$ and k_{wc} have similar physical meanings. However, the dimension of $E_{\mathrm{wc}}^{\mathrm{Eq}}$ is (N/mm^2) and the dimension of k_{wc} is (N/mm). Dimension of $E_{\mathrm{wc}}^{\mathrm{Eq}}$ is the same as compression strength, so $E_{\mathrm{wc}}^{\mathrm{Eq}}$ is selected as the first input parameter. In addition, the T changes with the layup of 2.5D woven composite plates. Thus, T is selected as the second input parameter.

Based on the observation of stress–strain curves in Fig. 4, the compression modulus before the ultimate failure load has slight nonlinear effects. Therefore, while the initial compression modulus $E_{\mathrm{wc}}^{\mathrm{Eq}}$ is assumed to be constant, Eq. (2) can be further rewritten as follows

$$\left[\sigma_{\mathrm{wc}}\right]_s = E_{\mathrm{wc}}^{\mathrm{Eq}} \left[\varepsilon_{\mathrm{wc}}\right]_f \tag{4}$$

Furthermore, based on the weaving scheme and thickness shown in Table 1, it can be found that as the layer number of cross-ply and angle-ply laminates increases, the nonlinear effect is gradually relieved. In other words, the thickness of the specimen directly reflects the information of the number of layers and ply angles and indirectly reflects the compression behaviors of the 2.5DWCPs. Thus, the thickness of specimen also strongly relates to $[\sigma_{\mathrm{wc}}]_s$.

To validate hypothesis mentioned above, the correlation analysis of the thickness, initial compression elastic modulus and strength of 2.5DWCPs is carried out. The expression of Pearson correlation coefficient matrix is presented in Eq. (5).

$$\begin{aligned} r(\mathbf{X},\mathbf{Y}) &= \frac{\sum_{i=1}^{n}\left(X_i - \overline{X}\right)\left(Y_i - \overline{Y}\right)}{\sqrt{\sum_{i=1}^{n}\left(X_i - \overline{X}\right)^2 \sum_{i=1}^{n}\left(Y_i - \overline{Y}\right)^2}} \\ \mathbf{R}(\mathbf{X},\mathbf{Y},\mathbf{Z}) &= \begin{bmatrix} r(\mathbf{X},\mathbf{X}) & r(\mathbf{X},\mathbf{Y}) & r(\mathbf{X},\mathbf{Z}) \\ & r(\mathbf{Y},\mathbf{Y}) & r(\mathbf{Y},\mathbf{Z}) \\ \text{syms} & & r(\mathbf{Z},\mathbf{Z}) \end{bmatrix} \end{aligned} \tag{5}$$

where n denotes the number of specimens, r ($\mathbf{X}$, $\mathbf{Y}$) denotes the Pearson correlation coefficient between $\mathbf{X}$ and $\mathbf{Y}$ vectors, $\mathbf{R}$ ($\mathbf{X}$, $\mathbf{Y}$, $\mathbf{Z}$) signifies the Pearson correlation coefficient matrix. In this work, $\mathbf{X}$, $\mathbf{Y}$ and $\mathbf{Z}$ respectively represent the thickness, initial compression elastic modulus and strength of specimens.

Figure 8a shows the scatter spatial distribution of specimen parameters. It can be found that both the initial compression modulus and thickness can clearly divide the 2.5DWCPs into five clusters of data points, which just verifies the potential physical relationship between the IPs and the OPs. What's more, the projections of Strength-Modules and Strength-Thickness graphs are also given, which is beneficial for visually capturing the relation between IPs and OPs. Figure 8b to g present Pearson correlation coefficient matrixes of A0, A1, B0, B1, C and all types of 2.5DWCPs. According to the results from Fig. 8b to f, it can be seen that the correlation between the initial compression elastic modulus and the strength is stronger than that between thickness and strength. The r ($\mathbf{Y}$, $\mathbf{Z}$) of type B1 2.5DWCPs reached a remarkable value of 0.921. Although the maximum absolute value of r ($\mathbf{X}$, $\mathbf{Z}$) for five types plates is just 0.4464, the correlation between the thickness and the initial compression elastic modulus r ($\mathbf{X}$, $\mathbf{Y}$) should be paid attentions to. Therefore, the initial compression elastic modulus has the potential to link the relationship between thickness and strength. In Fig. 8g, it is indicated that the dependences between the thickness/initial compression modulus and the strength are significant, which corresponds to the clear classification of the five types of 2.5DWCPs in Fig. 8a.

Finally, the initial compression modulus and thickness of specimens are selected as IPs, and the compression strength is selected as OP, so that the first ANNM for predicting compression strength in warp direction is established. For convenience of comparison, this model is subsequently abbreviated as the Direct Strength Prediction Model (DSPM).

The experimental data of one specimen is randomly selected for each type of 2.5DWCPs. Therefore, there are five experimental data in the test dataset. The remaining 24 experimental data are used as the training dataset. The programs written in Python language are applied to build an ANNM based on TensorFlow. The number of hidden layers is five and each layer has 64 neural nodes. The learning rate is 0.001. The ReLU [31] is selected as an activation function. The biggest advantage of the ReLU is that it can address the issue of disappearing gradients and speed up the training rate. Under the current neural network structure, the results of the training process are shown in Fig. 9. The Loss and ValLoss denote the loss value of the training dataset and validation dataset, respectively. The ratio of the validation dataset to the training dataset is 0.2. The Mean Square Error (MSE) is selected as the loss function to evaluate the performance of the DSPM.

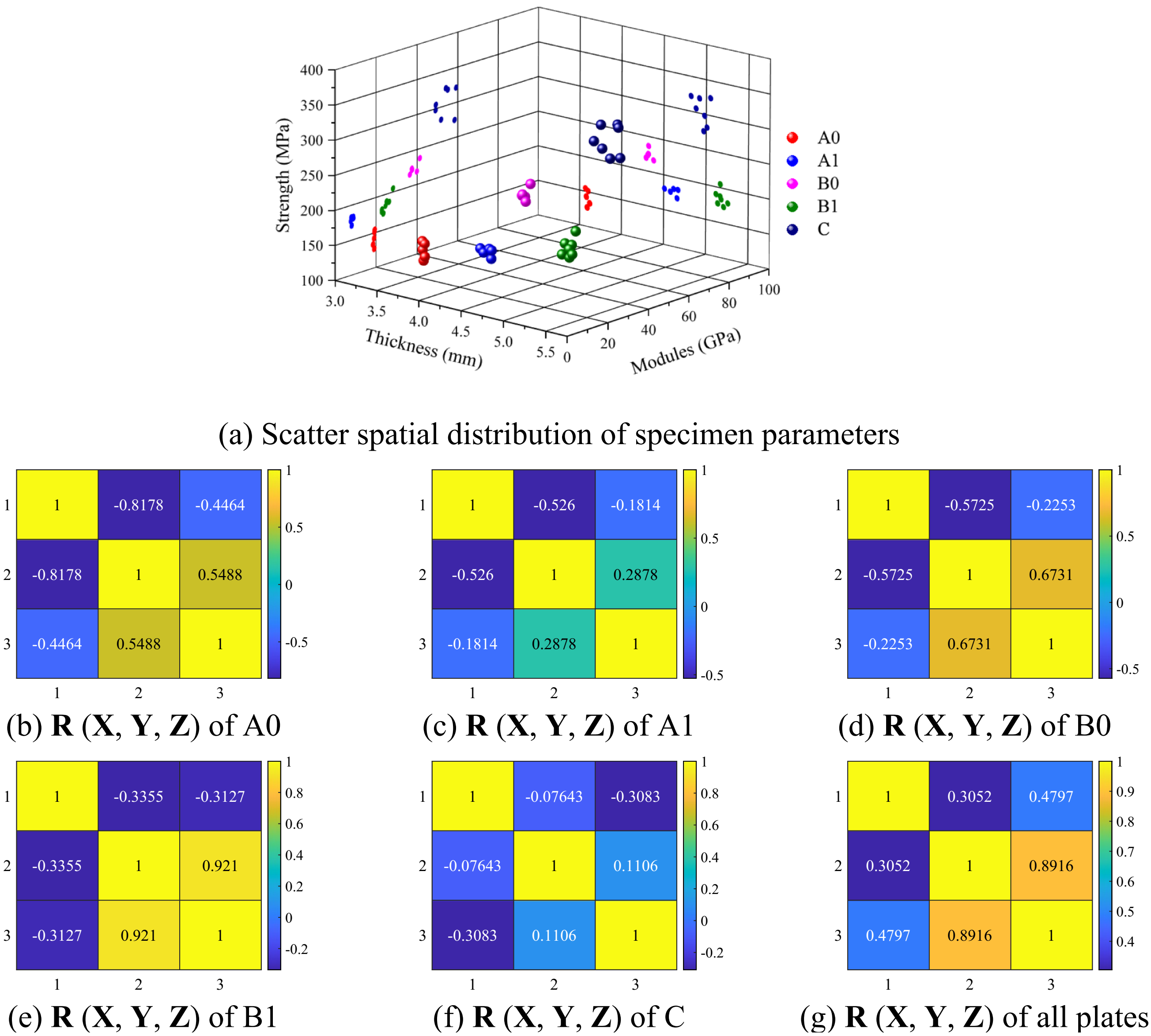

Fig. 8 Correlation analysis of IPs and OPs for ANNM (Tips: Row and column 1,2,3 represent the thickness, initial compression modulus and strength)

$$\mathrm{MSE} = \frac{\sum_{i=1}^{n}\left(Y_{\mathrm{real}} - Y_{\mathrm{predict}}\right)^2}{n} \tag{6}$$

where Y_{real} and Y_{predict} represent experimental data and predicted results of the model, respectively. n signifies the number of training dataset or test dataset. It is obvious that Loss and ValLoss converge quickly during the training process as shown in Fig. 9. When the ValLoss does not decrease for 10 consecutive steps, the iteration will be terminated. The number of iterations is 132. The total training time of the DSPM is 6.2s.

To show data flow process of the DSPM, the details on data preparation, data structure construction, data processing, the set of initiation and callback options for ANNM are elaborated in Fig. 10. The IPs can be found in Figs. 2b and 5a, and the OPs can be found in Fig. 5b. Finally, the compressive strengths for randomly selected specimens are predicted by the trained model.

3.3 Stress–Strain Curve Prediction Model

The model established in Sect. 3.2 directly utilizes the initial compression modulus and thickness of specimens to predict

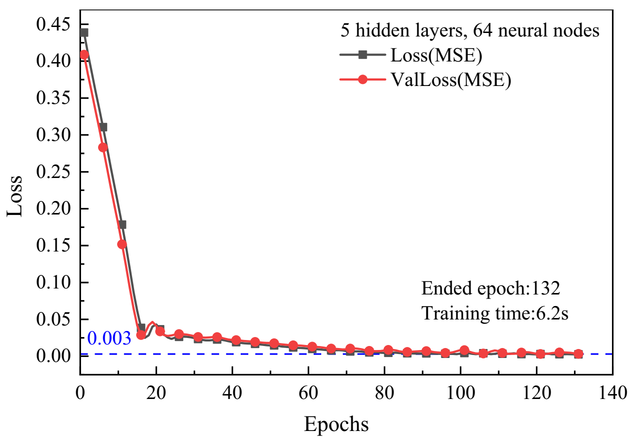

Fig. 9 Training results of the DSPM in warp direction

the compression strength of 2.5DWCPs. This section will introduce another prediction model. Except the initial compression modulus and the thickness of the specimen, the strains obtained from strain gauges are added as the third IPs. What's more, the OPs also change from compression strength to stresses. Until now, the second ANNM to predict stress–strain curve has been established.

The stress–strain curves predicted are utilized to indirectly obtain compression strength and failure strain in warp direction. The model is subsequently abbreviated as the Indirect Strength Prediction Model (ISPM). As presented in Fig. 4, the data points of the stress–strain curve are abundant. Compared with the DSPM predicting the compression strength directly, the ISPM predicting the compression strength indirectly can obtain a large number of training dataset from experimental data. The prediction accuracy of the ISPM based on ANNM is expected to improve significantly.

As shown in Fig. 4, the load drop phases of A0, B0 and B1 in Fig. 4a, c and d are gentle (Gradual Drop Mode, GDM), while the load drop phases of A1 and C in Fig. 4b and e are sudden (Sudden Drop Mode, SDM). In the process of training ANNMs, it is found that the sudden drop of stress near the failure strain may seriously interfere with the results predicted by ANNM. To illustrate the influences of GDM and SDM on prediction of stress–strain curves, the differences between two modes can be clearly demonstrated in Fig. 11.

There are two main reasons for this phenomenon: (1) The ultimate stress and initial stiffness of the same type 2.5DWCPs are similar. However, the failure strain is sometimes different. In the ISPM, the specimens with large failure strain fail at an earlier stage, and tracking accuracy of the elastic modulus nonlinear effect is also reduced. This results in a significant underestimation of the failure strength. However, it is inevitable in randomly initializing the training dataset and test dataset; (2) The stress gradient near the ultimate stress is discontinuous. It is difficult for ANNM to converge and capture gradient drop accurately. In addition, the issue of overfitting is easy to occur in data regression.

The SDM obviously makes the ISPM obtain wrong failure point, which results in large errors between predictions and original compression strength/failure strains. To address these issues, a new State Variable (SV) is introduced as OPs. The specific definition of SV is presented in Eq. (7).

$$\mathrm{SV} = \begin{cases} 1, & \boldsymbol{\varepsilon} \le \max(\boldsymbol{\varepsilon}) \\ 0, & \boldsymbol{\varepsilon} > \max(\boldsymbol{\varepsilon}) \end{cases} \tag{7}$$

where $\boldsymbol{\varepsilon}$ denotes the strain vector and $\max(\boldsymbol{\varepsilon})$ denotes failure strain corresponding to maximum stress. At the same time, the original stress vector is corrected by SV. The modified stress data can be obtained by Eq. (8).

$$\boldsymbol{\sigma}_{\mathrm{Modify}} = \mathrm{SV} \times \boldsymbol{\sigma}_{\mathrm{Real}} \tag{8}$$

where $\boldsymbol{\sigma}_{\mathrm{Real}}$ and $\boldsymbol{\sigma}_{\mathrm{Modify}}$ signify compression stresses before and after treatment.

Fig. 10 Training process of the DSPM

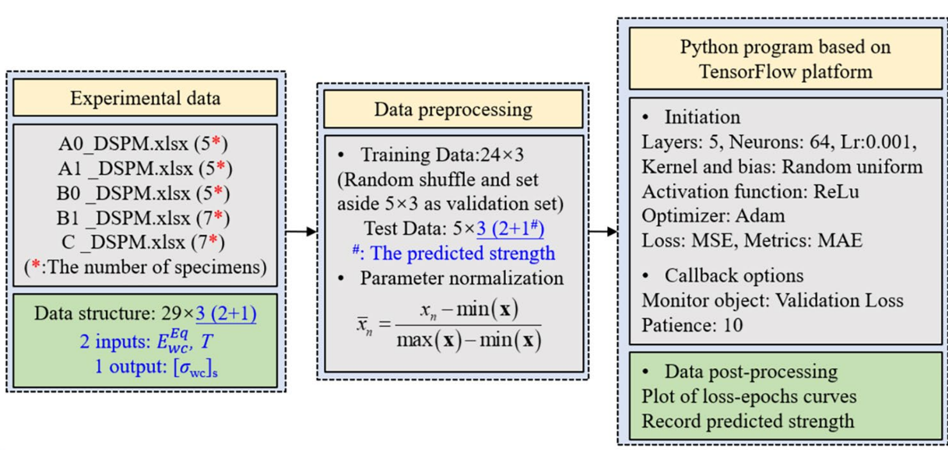

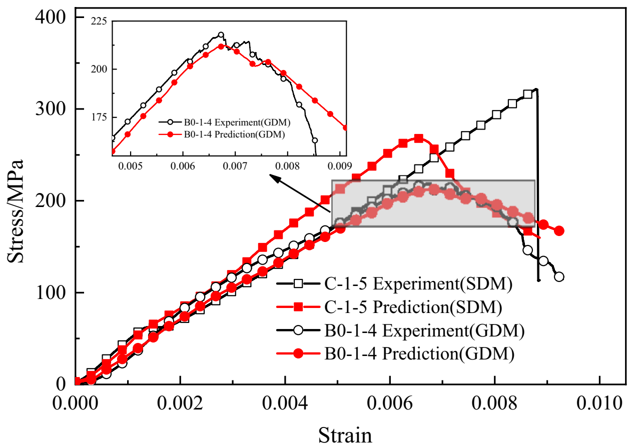

Fig. 11 The effect of GDM and SDM on prediction of stress–strain curves

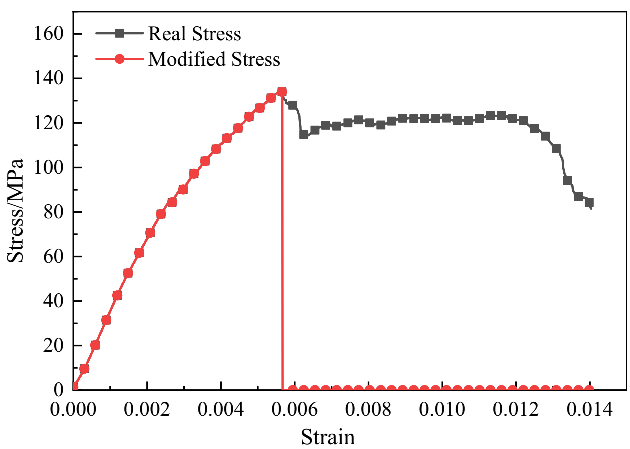

Fig. 12 Modified stress–strain curve of A0–1–3

The stress–strain curve of A0–1–3 modified by SV is shown in Fig. 12. The modified stress–strain curve directly abandons the data points of the load drop phase. However, the most concerned maximum stress and failure strain in engineering analysis are preserved more precisely. The modified stress–strain curve significantly reduces the training difficulty of the ANNM. In addition, the demand for the size of training data structure is greatly decreased.

There are 29 stress–strain curves of compression experiments in warp direction. The nine stress–strain curves (1, 1, 1, 3, 3) are randomly selected as test dataset in 2.5DWCPs (A0, A1, B0, B1, C), which means that the remaining 20 groups of experimental data are divided into training dataset. The programs are written in Python based on TensorFlow.

The learning rate is 0.001. The ratio of the validation dataset to the training dataset is 0.2. When the ValLoss does not decrease for 15 consecutive steps, the iteration will be terminated. The commonly used ReLU is selected as activation function. To improve the computational efficiency of the modified ISPM and prevent the gradient from vanishing and exploding, it is necessary to normalize the IPs and OPs as Eq. (9).

$$\begin{aligned} \overline{\mathrm{IP}} &= \frac{\mathrm{IP} - \min(\mathrm{IP})}{\max(\mathrm{IP}) - \min(\mathrm{IP})} \in [0,\ 1] \\ \overline{\mathrm{OP}} &= \frac{\mathrm{OP} - \min(\mathrm{OP})}{\max(\mathrm{OP}) - \min(\mathrm{OP})} \in [0,\ 1] \end{aligned} \tag{9}$$

where max/min represent the maximum/minimum value of IPs and OPs, which normalizes the raw data to [0, 1].

Since the training data size of the modified ISPM is much larger than that of the DSPM, it is necessary to complete the convergence analysis of the training model. The 16 neural network models with different scales are prepared for training, which has a combination of 3/6/9/12 hidden layers and 16/32/64/128 neural nodes in each layer. The convergence analysis of the modified ISPM is shown in Fig. 13.

It is obvious that the loss function MSE of model basically shows a gradually decreasing trend with the number of training parameters increasing. The MSE value of the smallest scale model is 0.0208 (3 hidden layers, 16 neural nodes in each layer, 914 parameters in total). The MSE value of the largest scale model is 0.0040 (12 hidden layers, 128 neural nodes in each layer, 198,914 parameters in total).

In order to better explain the discrepancy between the training results of different scale models, the loss function MSEs of the training dataset converges with the number of iterations are given in Fig. 14a. What's more, the predicted stress–strain curves of B1–1–6 in different scaled models are compared with the experimental data in Fig. 14b. The following conclusions can be drawn from observation: (1) The model (128 × 12), which has 128 neural nodes and 12 hidden layers, possesses the best convergence rate and prediction results; (2) The 64 × 9 model has no ability to capture the stress–strain curve after reaching the first stress peak. Third, near the first stress peak, the stress predictions of the 32 × 6 and 16 × 3 models are completely distorted. This can be attributed to the limited characterization of model parameters and the overfitting problems caused by too many iterations.

Finally, the number of hidden layers is 12 and each layer has 128 neural nodes. The results of stress–strain curves predicted by the modified ISPM are shown in Fig. 15. Compared with the DSPM, the modified ISPM utilizes a more effective training dataset from compression experiments. Accordingly, the structure of the network in the ISPM is relatively complex, which is beneficial to build the nonlinear

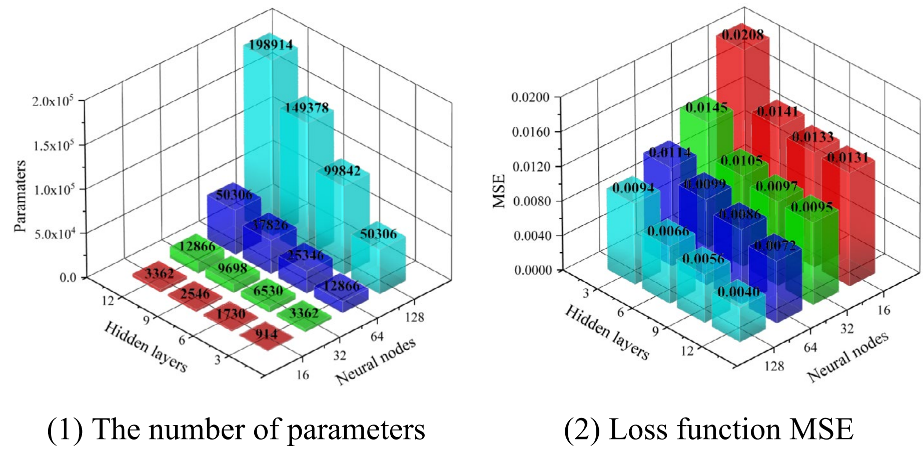

Fig. 13 The convergence analysis of the modified ISPM

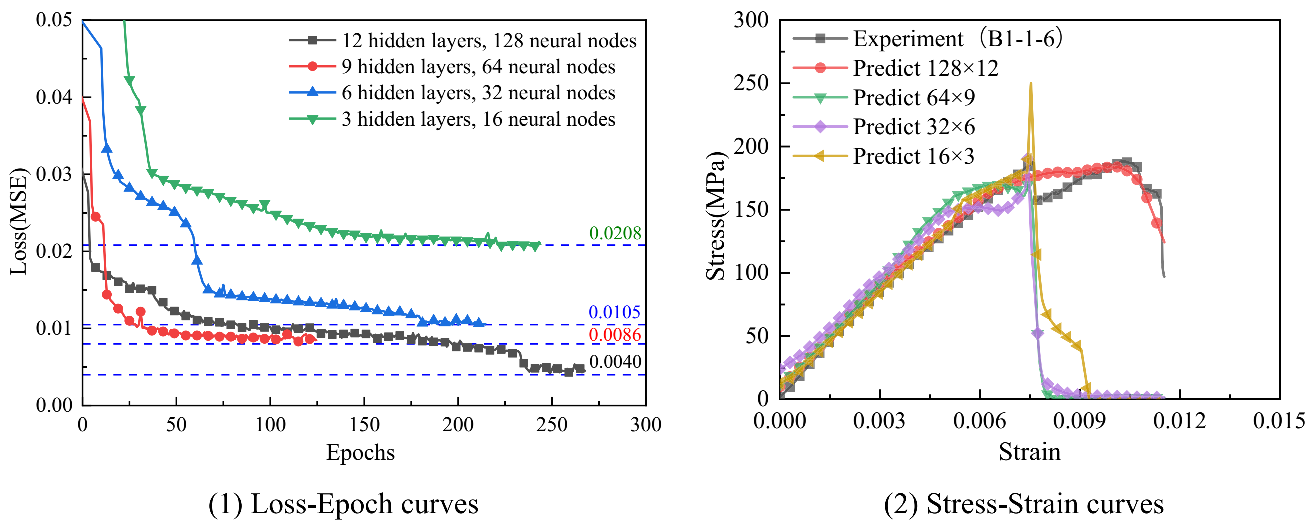

Fig. 14 Prediction of the modified ISPM with different neural network scales

relationship between stresses and strains. However, the convergence rates of TrainLoss and ValLoss are relatively slow during the training process. The number of iterations is 268. The total training time of the modified ISPM is 231s.

To show the data flow process of the modified ISPM, the details on data preparation, data structure construction, data processing, the set of initiation and callback options for ANNM are elaborated in Fig. 16. The IPs can be found from Figs. 2b, 5a and strain values in Fig. 4a ~ e, and the OPs can be found from stress values in Fig. 4a ~ e and modified stress-coordinates in Fig. 12. Then, the corresponding stresses for the randomly selected experimental strains are predicted by trained model. Finally, the stress–strain curves are obtained by plotting points of the test dataset. In addition, the maximum stress (compression strength) and failure strain can also be extracted.

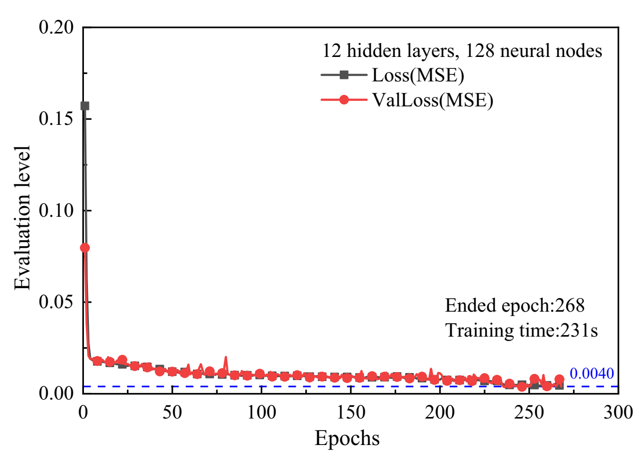

Fig. 15 Training results of the modified ISPM in warp direction

Fig. 16 Training process of the modified ISPM

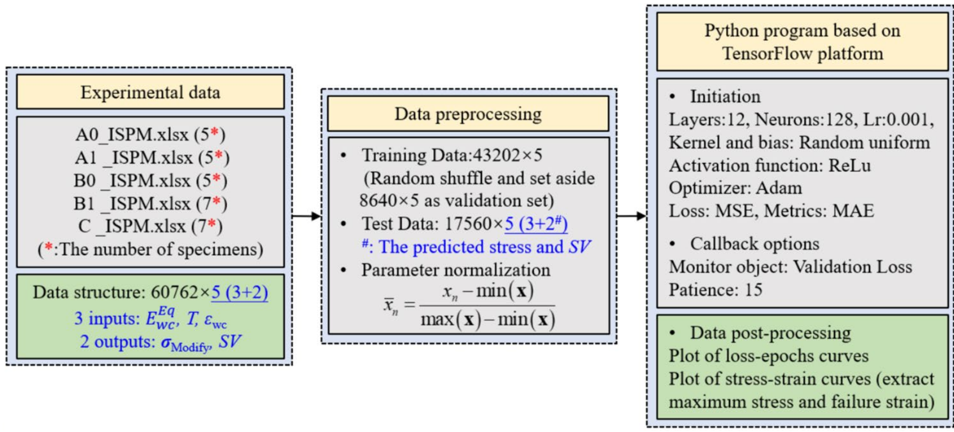

Table 2 The predicted compression strength in warp direction by the DSPM

Specimen ID	Real strength/MPa	Predicted strength/MPa	Error/%
A0–1–3	134.103	150.670	12.354
A1–1–2	170.573	150.239	– 11.921
B0–1–2	217.321	221.878	2.097
B1–1–4	183.670	202.018	9.990
C–1–3	277.949	308.774	11.090

4 Results and Discussion

4.1 The Results Predicted by the DSPM

The first ANNM selects the initial compression modulus and thickness of specimen as IPs, which directly outputs the compression strength in warp direction for five different kinds of 2.5DWCPs. After the training model, five test dataset are predicted by using the DSPM. The predicted results are shown in Table 2. The minimum percentage error between predictions and experimental strength is about 2.1%, and the maximum percentage error is about 12.4%. The results preliminarily validate the feasibility of ANNM to predict the compression strength of 2.5DWCPs. In theory, the prediction accuracy of the model can be further improved by expanding the size of the training dataset. However, the increase of specimens directly leads to an increase in the experimental cost. Therefore, although the DSPM is enough simple and direct to predict the compression strength, the prediction accuracy and cost–benefit ratio may not satisfy the actual demand for investigators. However, only the thickness and the initial compression elastic modulus are required for IPs, which means that it is non-destructive for strength prediction. It is more suitable for engineering application.

4.2 The Results Predicted by the ISPM

The second ANNM selects the initial compression elastic module, thickness and strains as IPs, which outputs stresses and indirectly calculates the compression strength in warp direction for five different 2.5DWCPs. After the training model, 9 test dataset are predicted using the modified ISPM. The predicted results are shown in Fig. 17. The results show that the predicted stress–strain curves are in good agreement with the experimental stress–strain curves.

Compared with the results in Fig. 11, the modification on real stresses which is demonstrated in Fig. 12 can significantly improve the accuracy of the predicted stress–strain curves with the sudden drop of stress. Furthermore, the characteristics of the ISPM are highlighted, which mainly focuses on compression strength and failure strain.

From the experimental data shown in Fig. 4, it can be concluded that the 2.5DWCPs A1 and C fail immediately when the stress–strain curves reach the maximum stress. After the modified stress–strain curve is substituted into the ANNM for training, the stress–strain curve predicted by the modified ISPM is in good agreement with experimental data. By contrast, the 2.5DWCPs A0, B0 and B1 fail gradually when the stress–strain curves reach the failure strain. Although the modified ISPM has no ability to predict the load drop phase of the real stress–strain curve, the predicted stress–strain curve accurately contains the maximum stress $\boldsymbol{\sigma}_{\max}$ and failure strain $\boldsymbol{\varepsilon}_{\max}$. The characteristics of the modified ISPM are more in line with the actual requirements of engineering practice.

Based on the stress–strain curves predicted by the modified ISPM, the compression strength in warp direction for five types of 2.5DWCPs can be indirectly computed by maximum stress and geometry dimension of specimens. The percentage errors between predicted and experimental compression strength/failure strain are presented in Table 3.

The results indicate that the maximum absolute error of predicted compression strength in warp direction is 5.623%,

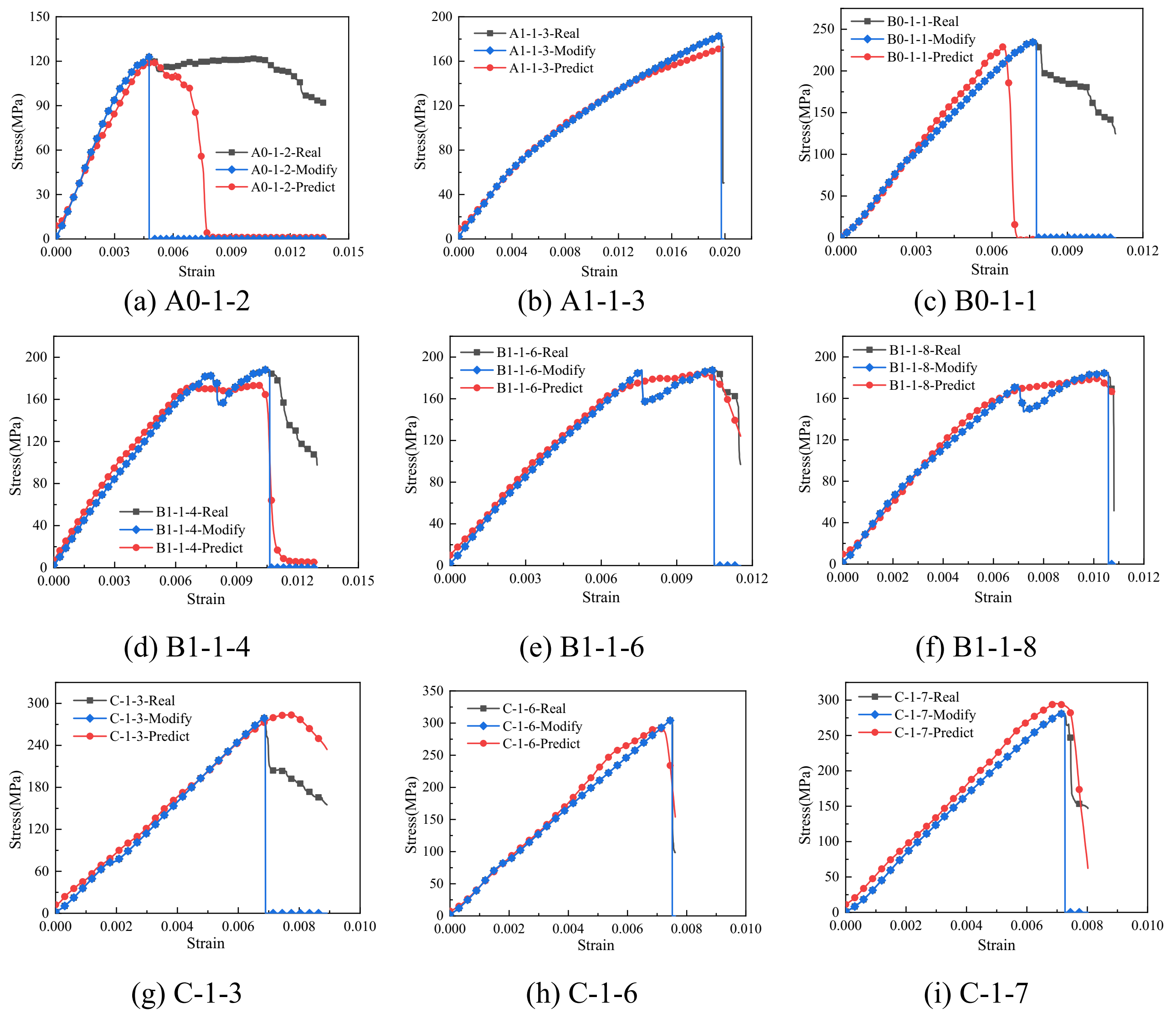

Fig. 17 The results of stress–strain curves predicted by the modified ISPM

and the maximum absolute error of predicted failure strain is 13.588%. From the stress–strain curves of B0 shown in Fig. 4c, the compression strength and failure strain of B0–1–1 are significantly different from those of the other four specimens. Therefore, it can be considered that the randomness of the training dataset and test dataset lead to undesired errors in the prediction of the failure strain. However, combined with the correlation analysis of the initial compression elastic modulus and compression strength in group B0 from Fig. 8, the input compression elastic modulus increases the ultimate stress and further improves the prediction accuracy of compression strength for B0–1–1. These results will verify the correlation between IPs and OPs of the ANNM, which also validate the performance of the modified ISPM.

To sum up, the modified ISPM has good performance after training with only 20 experimental data. The model can simultaneously obtain the compression strength and failure strain in warp direction, and it also has good prediction accuracy. What's more, the number of specimens and the dispersion of experimental data are also important factors affecting the results of the modified ISPM. Therefore, in the case of better stability of experimental data, the number of specimens in the training dataset can be further reduced, which can decrease the experimental costs.

4.3 Comparison Analysis Between DSPM and ISPM

The efficiency of the building model can be clearly demonstrated by comparing the training results of the DSPM and ISPM shown in Figs. 9 and 15. It can be found that the IPs

Table 3 The percentage errors between experimental data and prediction of the modified ISPM

Specimen ID	Real strength/MPa	Predicted strength/MPa	Absolute error/%	Real ε_{max}	Predict ε_{max}	Error/%
A0–1–2	123.050	118.905	3.369	0.00471	0.00491	4.246
A1–1–3	182.884	172.712	5.562	0.01963	0.01992	1.148
B0–1–1	236.334	229.163	3.038	0.00758	0.00655	13.588
B1–1–4	183.670	173.342	5.623	0.01045	0.01008	3.541
B1–1–6	187.662	183.941	1.983	0.01048	0.01005	4.103
B1–1–8	184.958	179.449	2.979	0.01057	0.01025	3.027
C–1–3	277.949	283.618	2.040	0.00688	0.00759	10.320
C–1–6	305.601	292.618	4.249	0.00748	0.00701	6.283
C–1–7	281.903	295.131	4.692	0.00717	0.00696	2.929

and OPs of the DSPM are more straightforward than those of the ISPM. Therefore, the construction and training of the DSPM are easier and the convergence rate is relatively faster.

By comparing the results predicted by the original ISPM and modified ISPM in Figs. 11 and 17, the modified model has three significant advantages over the original model. (1) The introduced *SV* essentially reduces the size of the training dataset because the modified stress is zero when the strain reaches the failure strain. The experimental data points after the failure of 2.5DWCPs can be appropriately deleted; (2) The SV enables an accurate capture of ultimate stress and failure strain, which highlights the characteristics of experimental data and further reduces the requirement for the size of the training dataset. It is expected to reduce experimental costs; (3) The SV can effectively improve the prediction accuracy of failure points in stress–strain curve with sudden stress drop, which prevent the underestimation of ultimate stress by the original ISPM.

By comparing the results predicted by the DSPM and the modified ISPM in Tables 2 and 3, the construction of the modified ISPM is relatively complex and the training process of the modified ISPM is more time-consuming than the DSPM. However, the modified ISPM can predict the compression strength and failure strain in the warp direction, and the predicted results are in good agreement with experimental data. Compared with the issues of parameters dependence, complex modeling and analysis in FEMs, the modified ISPM can efficiently and accurately predict compression strength and stress–strain curve.

5 Conclusions

In this paper, 29 quasi-static compression experiment data in warp direction of 2.5DWCPs are utilized to construct two different ANNMs. The first DSPM inputs the initial compression elastic modules and thickness, and outputs compression strength in warp direction. The second modified ISPM inputs the initial elastic compression modules, thickness and strains, and outputs stresses and SV. Two proposed ANNMs are validated by using the test dataset. By analyzing the predicted strength and stress–strain curves of five types of 2.5DWCPs, the main observations and conclusions are summarized as follows:

(1) The IPs and OPs are simple and direct in the DSPM, which is easy to be constructed and trained. The prediction errors of compression strength range from 2.097 to 12.354%. Although the DSPM is less accurate than the ISPM, it is still proposed to predict mechanical properties when few experimental data are prepared.
(2) To prevent the underestimation of maximum stress by the original ISPM, the simplified data processing method is firstly proposed. The modified ISPM with SV obviously reduces data structure and time cost, which also improves the accuracy of predicting failure point in the stress–strain curve.
(3) The modified ISPM can obtain more training data from experiments than the DSPM. Thus, the predicted stress–strain curve is highly consistent with the experimental data. The prediction errors of compression strength range from 1.983 to 5.623%. Therefore, the modified ISPM has the potential to predict the stress–strain curves and compression strength of 2.5DWCPs by replacing the complex modeling and analysis of FEMs.

Acknowledgements The work described in this paper was supported by the National Key R&D Program of China [2022YFC2204500] and the National Natural Sciences Foundation of China [No. 12172295].

Declarations

Conflict of interest The authors declare that they have no known competing financial interests or personal relationships that could have appeared to influence the work reported in this paper.

References

1. X. Zhang, Y. Chen, J. Hu, Prog. Aeosp. Sci. **97**, 22 (2018). https://doi.org/10.1016/j.paerosci.2018.01.001
2. D.K. Rajak, D.D. Pagar, R. Kumar, C.I. Pruncu, J. Mater. Res. Technol. **8**, 6354 (2019). https://doi.org/10.1016/j.jmrt.2019.09.068
3. H.A. Aisyah, M.T. Paridah, S.M. Sapuan, R.A. Ilyas, A. Khalina, N.M. Nurazzi, S.H. Lee, C.H. Lee, Polymers **13**, 471 (2021). https://doi.org/10.3390/polym13030471
4. L. Chen, X. Yao, S. Cen, Compos. Pt. B-Eng. **74**, 53 (2015). https://doi.org/10.1016/j.compositesb.2015.01.009
5. L. Yuan, W. Fan, Y. Miao, J. Li, L. Xue, W. Dang, J. Dong, L. Wei, R. Sun, J. Ind. Text. **51**, 134 (2021). https://doi.org/10.1177/1528083719866937
6. H. Kang, P. He, Y. Dai, C. Zhang, Fiber. Polym. **20**, 2625 (2019). https://doi.org/10.1007/s12221-019-9328-7
7. J. Xie, C. Liu, Z. Yang, W. Jiao, Y. Zhang, X. Chen, L. Chen, J. Compos. Mater. **54**, 2529 (2020). https://doi.org/10.1177/0021998319899134
8. D. Zhang, L. Chen, Y. Wang, L. Zhang, Y. Zhang, K. Yu, X. Lu, J. Sun, X. Xiao, K. Qian, J. Mater. Sci. **52**, 6814 (2017). https://doi.org/10.1007/s10853-017-0921-0
9. A. Hallal, R. Younes, F. Fardoun, S. Nehme, Compos. Struct. **94**, 3009 (2012). https://doi.org/10.1016/j.compstruct.2012.03.019
10. L. Yao, Z. Liu, Q. Song, B. Wang, Y. Cai, Compos. Struct. **304**, 116448 (2023). https://doi.org/10.1016/j.compstruct.2022.116448
11. G. Liu, L. Zhang, L. Guo, F. Liao, T. Zheng, S. Zhong, Compos. Struct. **208**, 233 (2019). https://doi.org/10.1016/j.compstruct.2018.09.081
12. R. Younes, W. Zaki, Compos. Struct. **93**, 1255 (2011). https://doi.org/10.1016/j.compstruct.2010.10.013
13. J. Ma, Y. Xu, L. Zhang, L. Cheng, J. Nie, N. Dong, Scr. Mater. **54**, 1967 (2006). https://doi.org/10.1016/j.scriptamat.2006.01.047
14. G. Odegard, K. Searles, M. Kumosa, Mech. Adv. Mater. Struct. **7**, 129 (2000). https://doi.org/10.1080/107594100305348
15. S. Ogihara, K.L. Reifsnider, Appl. Compos. Mater. **9**, 249 (2002). https://doi.org/10.1023/A:1016069220255
16. O. Cousigné, D. Moncayo, D. Coutellier, P. Camanho, H. Naceur, S. Hampel, Compos. Struct. **106**, 601 (2013). https://doi.org/10.1016/j.compstruct.2013.07.026
17. Y. Wang, Y. Zhou, C. Jin, Compos. Struct. **296**, 115905 (2022). https://doi.org/10.1016/j.compstruct.2022.115905
18. H.T. Thai, Structures **38**, 448 (2022). https://doi.org/10.1016/j.istruc.2022.02.003
19. A. Sharma, T. Mukhopadhyay, S.M. Rangappa, S. Siengchin, V. Kushvaha, Arch. Comput. Method Eng. **29**, 3341 (2022). https://doi.org/10.1007/s11831-021-09700-9
20. K. Guo, Z. Yang, C.-H. Yu, M.J. Buehler, Mater. Horiz. **8**, 1153 (2021). https://doi.org/10.1039/D0MH01451F
21. K. Zhang, L. Ma, Z. Song, H. Gao, W. Zhou, J. Liu, R. Tao, Compos. Struct. **296**, 115835 (2022). https://doi.org/10.1016/j.compstruct.2022.115835
22. A. Sharan, M. Mitra, Modelling Simul. Mater. Sci. Eng. **30**, 075001 (2022). https://doi.org/10.1088/1361-651X/ac83df
23. D.W. Kim, M.-S. Go, J.H. Lim, S. Lee, Compos. Struct. **313**, 116902 (2023). https://doi.org/10.1016/j.compstruct.2023.116902
24. S. Gowid, E. Mahdi, F. Alabtah, Compos. Struct. **229**, 111473 (2019). https://doi.org/10.1016/j.compstruct.2019.111473
25. X. Liu, F. Gasco, J. Goodsell, W. Yu, Compos. Struct. **230**, 111505 (2019). https://doi.org/10.1016/j.compstruct.2019.111505
26. M. Halvaei, M. Jamshidi, M. Latifi, M. Ejtemaei, Constr. Build. Mater. **262**, 120877 (2020). https://doi.org/10.1016/j.conbuildmat.2020.120877
27. K. Hornik, M. Stinchcombe, H. White, Neural Netw. **2**, 359 (1989). https://doi.org/10.1016/0893-6080(89)90020-8
28. T. Qu, S. Di, Y. T. Feng, M. Wang, T. Zhao, M. Wang, Comp. Model. Eng. Sci. **128**, 129 (2021). https://doi.org/10.32604/cmes.2021.016172
29. S. Yan, X. Zou, M. Ilkhani, A. Jones, Compos. Pt. B-Eng. **194**, 108014 (2020). https://doi.org/10.1016/j.compositesb.2020.108014
30. D. Tong, R. Mintram, Int. J. Mach. Learn. Cybern. **1**, 75 (2010). https://doi.org/10.1007/s13042-010-0004-x
31. J. Yang, R. Xu, H. Hu, Q. Huang, W. Huang, Compos. Struct. **215**, 446 (2019). https://doi.org/10.1016/j.compstruct.2019.02.064